ORIGINAL ARTICLE

lajss.org© Latin American Journal of Solids and Structures

www.lajss.org

Behaviour of hollow circular section with multiple perforations under compression, flexure and torsion

Woo Yian Peen[a]

Choong Kok Keong[b]*

Omid Hassanshahi[b]

[a] Universiti Teknologi MARA (Penang), 13500 Permatang Pauh, Penang, Malaysia. E-mail: wooyianpeen@gmail.com
[b] School of Civil Engineering, Engineering Campus, Universiti Sains Malaysia, 14300 Nibong Tebal, Penang, Malaysia. E-mail: cekkc@usm.my, omid.hasanshahi@gmail.com

*Corresponding author

http://dx.doi.org/10.1590/1679-78255387

Abstract

Effect of the presence of perforations on thin structure has been extensively investigated for decades. Various perforation parameters were investigated in past studies. However, study on thin cylinder with multiple perforations has not been carried out. In searching for lighter structural members, the concept of perforated hollow section has been inspired by the shape and arrangement of multiple perforations observed in the Cholla skeleton. Effects of multiple perforation parameters on circular hollow section have been the main interest. This paper presents the verification of FEM simulation with test results. A non-perforated circular hollow section (control model) and a circular hollow section penetrated with 12 nos. of circular shape perforations in array arrangement were selected for the verification process. Both test specimen and FEA models were subjected to compression, flexural and torsional loads. For result comparison within the material linear range, FEA models show good agreement with test results for compression and flexural load cases, and for control models under torsional load case. For perforated models under torsional load, FEA results correspond well with the inclined strain gauge readings. FEM analysis method is considered capable to produce reliable result for loading within the material linear range for circular hollow sections with multiple perforations.

Keywords

Cholla skeleton, multiple perforated circular hollow section, experimental verification.

1 INTRODUCTION

Effect of the presence of perforations on thin structure has been extensively investigated for decades. It is commonly known that presence of hole significantly affected the structural responses, capacity and failure mode of a structure. Various perforation parameters were investigated in previous studies. Many studies investigated the effect of perforation dimension on the performance of plates (Paik, 2007, Shanmugam et al., 1999) and cylinders (Yeh et al., 1999, Han et al., 2006). Most of them focused on the width of the perforation except Ghazijahani et al. (2015) who studied the effect of perforation height. Some studies investigated the effect of the perforation shape (Shanmugam et al., 1999; Shariati and Rokhi, 2010; Ghazijahani et al., 2015; Shariati and Dadrasi, 2012). Comparisons were generally made between circular and square shaped perforations except Shariati and Rokhi (2010) where the study was on the effect of perforation aspect ratio for 'elongated shaped' perforations, and Ghazijahani et al. (2015) where the study was on the effect of different shapes of door shape perforation. Orientation of 'elongated' perforations was also studied on plate (El-Sawy and Nazmy, 2001, Maiorana et al., 2009) and cylinder (Shariati and Rokhi, 2010). Another

Received: November 15, 2018. In Revised Form: January 16, 2019. Accepted: January 18, 2019. Available online: January 21, 2019.
http://dx.doi.org/10.1590/1679-78255387

perforation parameter studied was the location of perforation (Yeh et al., 1999; Jullien and Limam, 1998; Han et al., 2006; El-Sawy and Nazmy, 2001; Shariati and Rokhi, 2008) where the position locations along the direction of loads were generally investigated.

The structural behavior studied are the buckling loads (elastic and ultimate) (Paik, 2007; Shanmugam et al., 1999; Jullien and Limam, 1998; Shariati and Rokhi, 2010; Han et al., 2006; Shariati and Dadrasi, 2012; Shariati and Rokhi, 2008), the bending buckling (Yeh et al., 1999), the structure's stability (El-Sawy and Nazmy, 2001), the structure's failure mode (Yeh et al., 1999) and the natural frequency of the structure caused by different fractions of multiple perforations with 'homogeneous' pattern on cylinder (Cousseau et al., 1998). Stress flow lines were also discussed in Ghazijahani et al. (2015) on how they were deflected when they met opening and how the deflected stress flow affected the strain values below the opening, with the development of the buckling.

Only a small amount of perforated hollow sections related to structural engineering domain were found: The Agridulce Lookout House XPIRAL (2009), a light weight perforated egg shape pod (Trendir, 2009, Kazuya, 2007), and The O-14 Tower (Lane, 2009, Reiser et al., 2010). From the cited literatures in the structural domain, most of the studies focused on structures with single perforation except the works by Cousseau et al. (1998) and Degtyarev and Degtyareva (2012). Studies on effect of multiple perforations are found to be scarce. Furthermore, there was lack of variability in perforation shape and patterns which have been studied. Constructed perforated hollow sections found so far have proven the possibility of multiple perforated hollow structures. However, no information about the multiple perforation parameters was found except the work of Cousseau et al. (1998).

In searching for lighter structural members, the concept of perforated hollow section has been inspired by the shape and perforations arrangement observed from the Cholla skeleton. These novel structural members can possibly be used in structural elements such as column, beam and building core where perforations are needed or desired either for functional or aesthetic purpose. Study on effects of multiple perforation parameters on structural behaviour of circular hollow section has been the main interest of the authors. However, we need to be able to evaluate the effect of multiple perforations on structural behavior. Fabrication of multiple perforated hollow sections with complex patterns is a difficult task. In order to understand the stress distribution on these perforated hollow sections, one of the methods which is versatile is FEM. However, FEM results need to be verified. This paper presents the verification of FEM simulation with results obtained from test on circular hollow section with multiple perforations.

2 VALIDATION OF PERFORMANCE OF PERFORATED CIRCULAR HOLLOW SECTION MODEL

Finite element software LUSAS (FEA Ltd, 2005) was used in the FEM simulation process. To verify the appropriateness of the models generated with LUSAS, comparison with the numerical and experimental results for a single perforated circular hollow section reported by Han et al. (2006) was first carried out. The selected model from Han et al. (2006) was T1_5D_7_50L as shown in Figure 1.

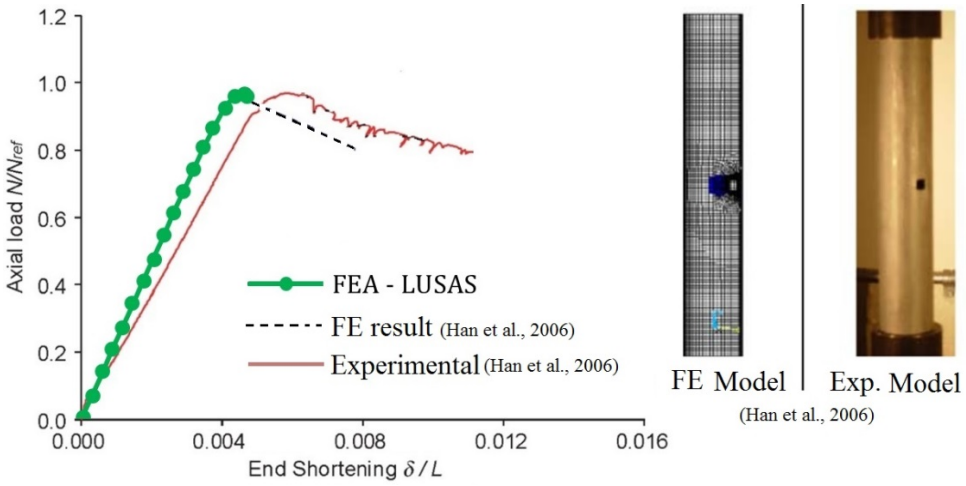

Figure 1: Comparison of LUSAS results with FE and experimental results by Han et al. (2006).

The perforated cylindrical shell was made of 6061-T6 aluminum alloys with the sheet rolling in the circumferential direction. Dimensions of the model are: H = 200 mm, D = 40 mm, and t = 0.889 mm. This cylindrical shell was penetrated with a rounded corner square opening (7.5 mm * 7.5 mm with 0.5 mm radius chamfered at corners) at its

mid-height and was subjected to axial compression load. The material properties for the model are: E = 68.948 GPa, ν = 0.33, and σ_y = 276 N/mm^2. The multi-linear isotropic hardening constitutive model which represents the uniaxial stress-strain behaviour of the material is shown in Table 1.

Table 1: Stress-strain behaviour of multi-linear material model.

Stress (MPa)	0.000	275.792	278.848
Strain	0.000	0.004	0.005
Stress (MPa)	284.473	306.299	310.395
Strain	0.012	0.051	0.069

The selected model was generated by the authors with similar dimensions and material properties. 8-node thin shell was used to model the cylindrical surface. The unloaded end of the cylindrical shell was restrained in all translational and rotational movements while the translational movement in model longitudinal direction was unrestrained. The model was assigned with a prescribed displacement at the loaded end.

Loading (N) and end shortening (δ) were gathered from LUSAS simulation results. The main focus for this verification process is within the elastic range up to the yield point. Loadings (vertical axis) at each stage were normalized with N_{ref} = 276*0.889 = 245.36 N/mm, and the corresponding end shortenings (horizontal axis) were normalized with the model length (200 mm). Comparison of LUSAS results and results of Han et al. (2006) is shown in Figure 1. The curve for LUSAS results correlates well with results of Han et al. (2006), specifically with the FE result (simulated with ANSYS) for the range up to the yield point. This indicates that modeling of the perforated hollow cylindrical section is appropriate and analysis results using LUSAS is acceptable. Based on this satisfactory validation with previous work by Han et al. (2006), the study was then proceeded to cases of hollow cylindrical section with multiple perforations.

3 MULTIPLE PERFORATED HOLLOW CYLINDER TEST SPECIMEN AND TEST SET-UP

A non-perforated circular hollow section (control model) and a circular hollow section penetrated with 12 nos. of circular shape *(C)* perforations (with diamater of 34mm) in array arrangement (*AR*) (3 layers and 4 perforations per layer), and with 10% of perforations to model surface area (*AR*/10/3-4(*S*)/C/ϕ34) were used for the verification process. Overall dimensions of the test specimens were decided based on the availability of raw material (circular hollow section) in the market, and the capacity (volume and loading) of testing machine. The verification was carried out for compression, flexural and torsional load cases individually. These three basic types of loading were considered separately due to the reason that the main aim of this study is to investigate effect of multiple perforations in a hollow cylinder under compression, flexure and torsion first. After basic understanding on performance under individual loading case with verification using test result, combined loading effect can be further studied.

3.1 Test specimens

Shimadzu UH-F1000KN Universal Testing Machine (UTM) was used for the tests. Kyowa UCAM-60B data logger was used to record the digital data from all the strain gauges. Instron-8802 UTM was used to carry out tensile tests. Material properties obtained from tensile tests were input into LUSAS for FEA simulation. FEA models were generated according to the actual dimensions and loading magnitudes as used in the test specimens.

The raw material for test specimen fabrication was selected among Grade B seamless API 5L plain-end line pipe. The original pipe outer diameter is 114.3 mm with 8.56 mm of wall thickness. The original thickness is sufficient to resist shear force generated at the loaders and supports during flexural and torsional tests without localized deformation. Total length for the test specimens are: 350 mm for compression test specimens; 1400 mm for 4-point bending test specimens; and 650 mm for torsional test specimens. Portion to be tested is the 300 mm length of middle stretch of each test specimen. The 300 mm middle stretch of the test specimens was lathed to smaller desired thicknesses (3.6mm for compression and flexural tests; 3.2 mm for torsional test) with lathe machine. Perforations were cut using machines equipped with computerized numerical control (CNC) technique. Tensile coupons with 25 mm width, 300 mm length and 3.6 mm thickness were cut from one of the lathed API pipes. The test specimens for each load test are shown in Figure 2. Three specimens were tested for each load case. The specimen markings are denoted as CC01 to CC03 and CP01 to CP03 for control and perforated compression test specimens; FC01 to FC03 and FP01 to

FP03 for control and perforated flexural test specimens; and TC01 to TC03 and TP01 to TP03 for control and perforated torsional test specimens.

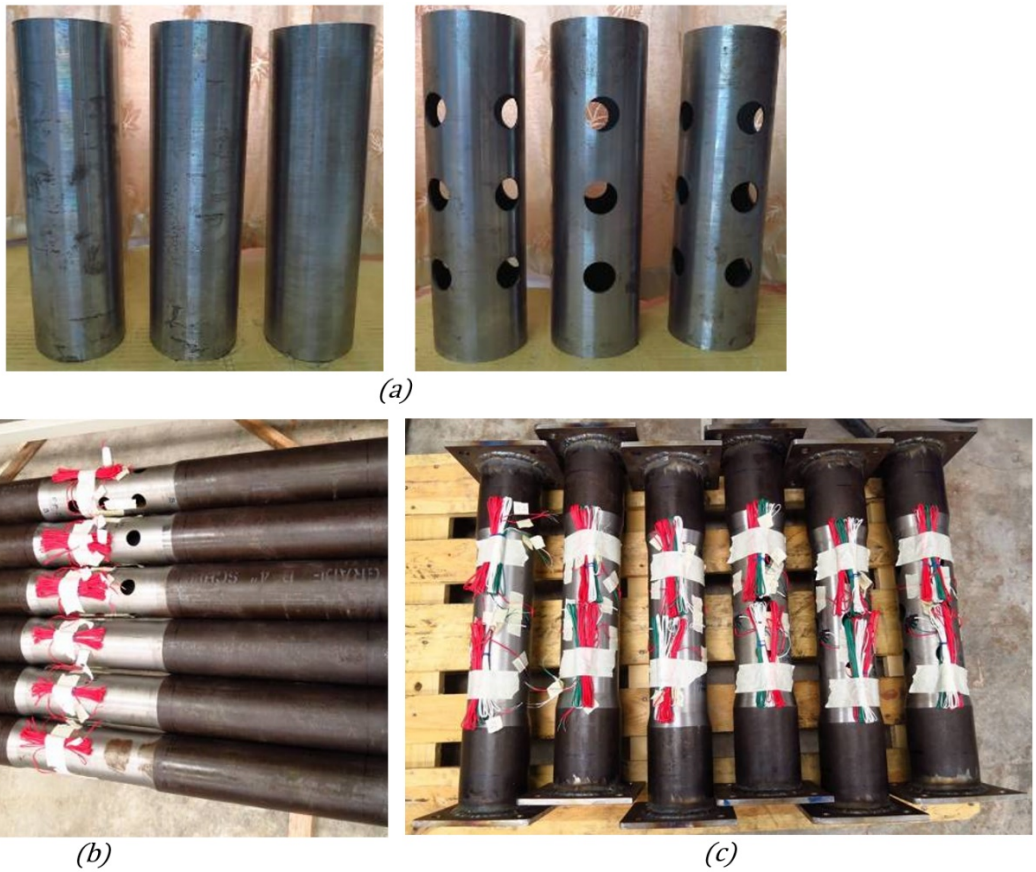

Figure 2: Test specimens, (a) compression test specimens, (b) flexural test specimens, (c) torsional test specimens.

3.2 Test set-up

Figure 3 shows the set-up used for laboratory testing. Compression specimens were lathed to the full length. The specimens were tested like normal compression tests carried out using UTM. Two LVDTs (Linear Variable Differential Transformer) were installed at orthogonal axes of each specimen to monitor the specimen buckling (Figure 3a).

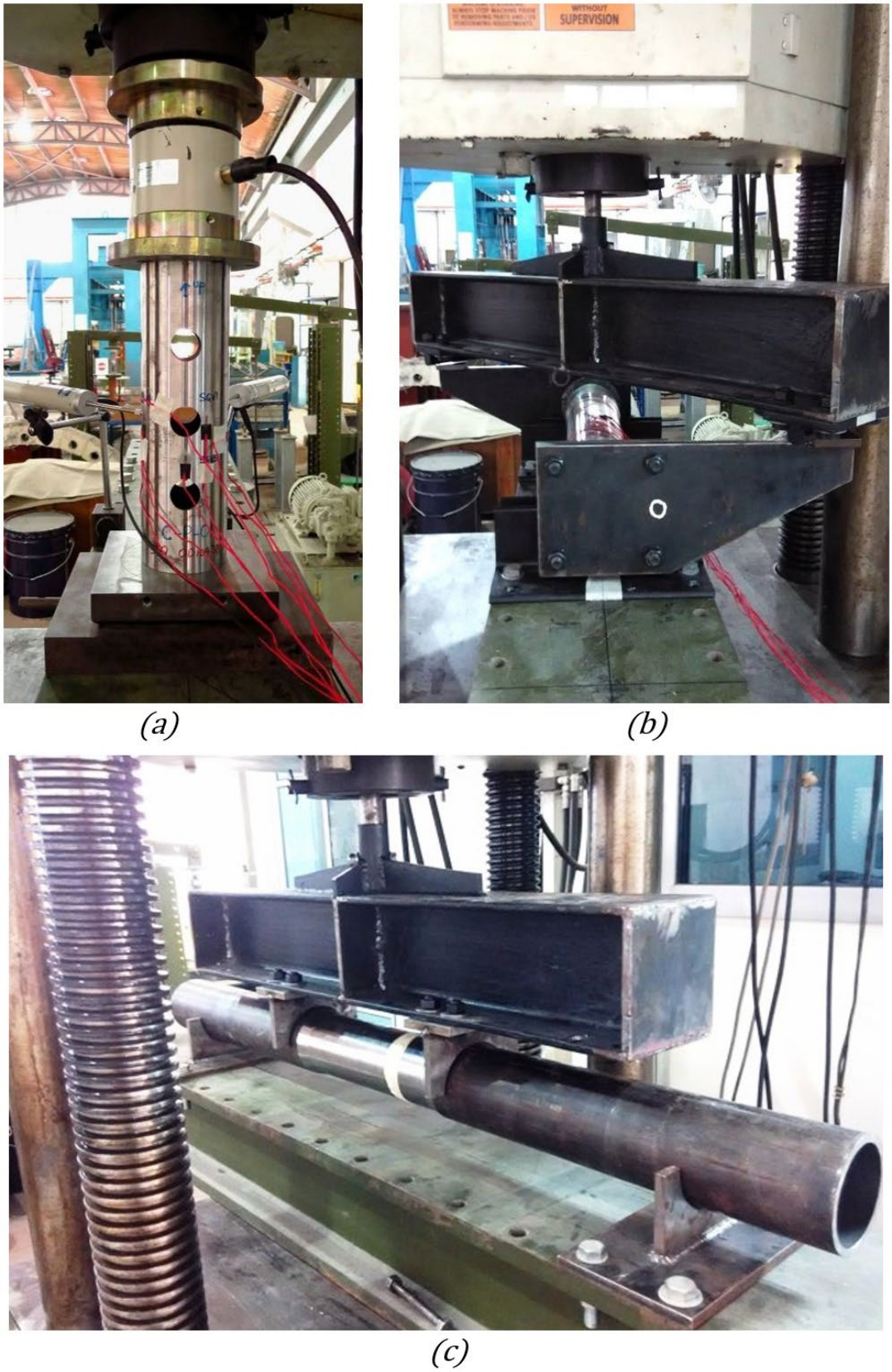

Figure 3**:** *Experimental set-up for (a) compression test, (b) torsional test and (c) flexural test.*

4-point bending method was adopted to generate pure flexural load on test specimens. A 1 m spreader beam (152x152x30 kg/m UB) connected with a 30 mm diameter steel rod, was clamped at the upper part for the installation of loaders. Distance between loaders was set to be 400 mm. At the lower part, the 1400 mm flexural specimens were rested on two supports (Figure 3c).

To create twisting effect from the UTM, the spreader beam which was clamped at the upper part of the UTM was tilted about 42° in counter-clockwise direction. Loader bars were installed on the spreader beam with approximately 500 mm apart. For the 650 mm long torsion specimens, 10 mm mild steel plates were welded to both ends of the pipe. Torsion arms (16 mm thick) were connected to the end plates. 4 nos. of HSFG (high strength friction grip) bolts were fastened at each connection to prevent slippage during the twisting of the specimens. Rotatable supports were placed 500 mm apart and were located close to the end plates. The supports were located as close as possible to the loading point in order to minimize the bending effect on the specimens. Buffers were provided to prevent clashing of bolts between the supports and torsion arms (Figure 3b).

Strain gauges and strain rosettes (with 0°/45°/90° arrangement) were used to obtain the strain data of the specimens at the prescribed locations during tests. Figures 4, 5 and 6 show the locations of strain gauges and rosettes on the physical specimens for compression, flexural and torsional load case, respectively. By assuming that the principal strain is oriented at 45° to the longitudinal axis which corresponds to z-axis, two strain gauges on each model were installed at approximately 45° to the longitudinal axis (Figure 6) with the purpose to directly record the principal major and minor strains. Orientation of strain rosettes (direction 1, 2 and 3) used in specimen for torsional load case is also indicated in Figure 6.

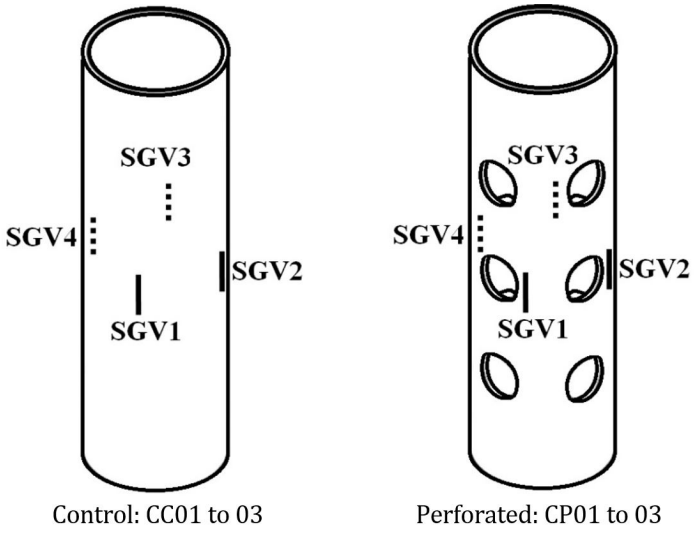

Figure 4**:** *Locations for strain gauge (Specimens for compression test).*

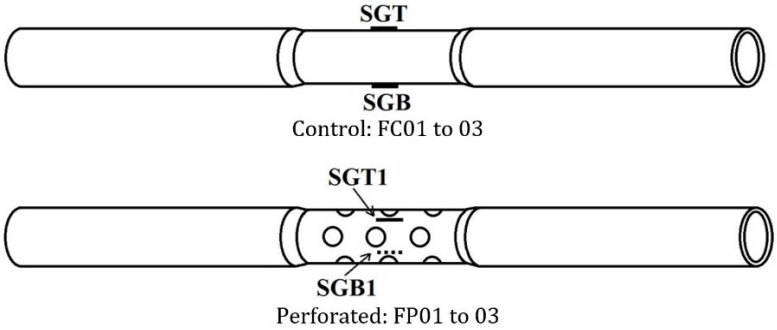

Figure 5**:** *Locations for strain gauge (Specimens for flexural test).*

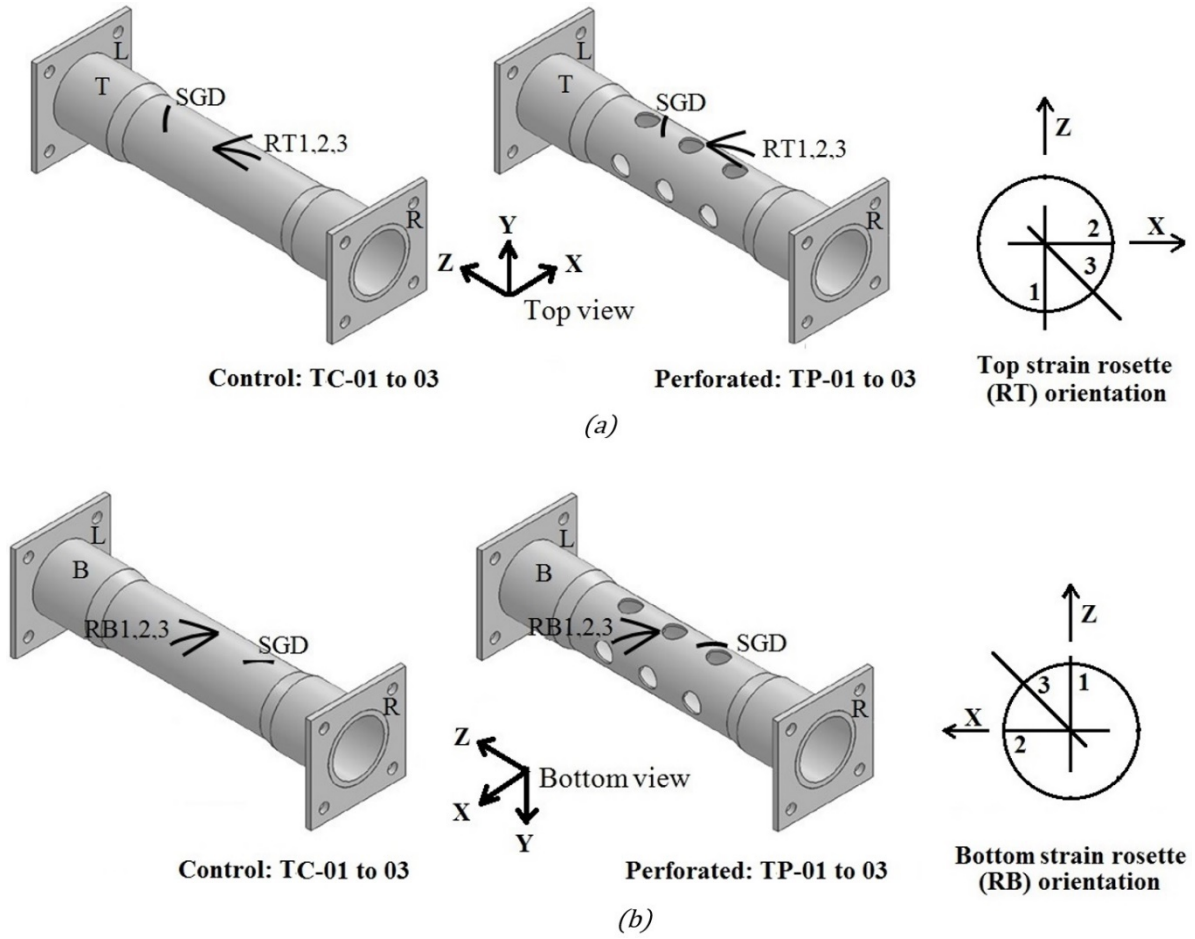

Figure 6: *Locations for strain gauges (Specimens for torsional test), (a) top view, (b) bottom view.*

Tensile tests were carried out using INSTRON-8802 UTM on tensile coupons. The average value obtained for modulus of elasticity (E = 175 GPa), Poisson's ratio (v = 0.21) and yield strength (σ_y = 322 MPa) were used as the material properties for the FEA verification models. A simplified stress-strain curve (as shown in Figure 7) was incorporated in LUSAS to cater for material nonlinearity in the analysis.

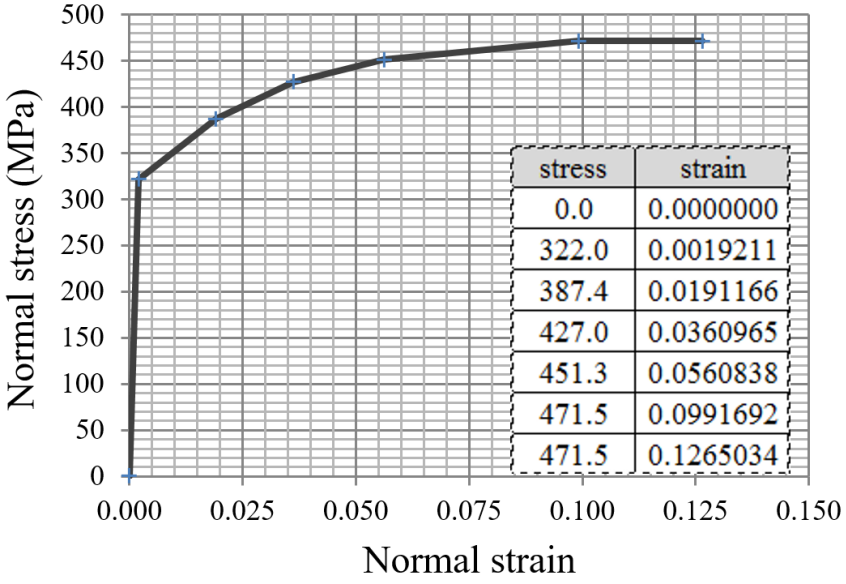

Figure 7: *Simplified stress-strain curve for FEA models*.

4 COMPARISON BETWEEN FEA AND TEST RESULTS

Nodes for the FEA models which approximate the locations of the strain gauges on test specimens were identified. Strains were obtained from these nodes and comparison was made with strains recorded for test specimens.

4.1 Computational Analysis

The generation and analysis of computational models were carried out for the control model and perforated model using finite element software LUSAS. Material behaviour obtained from tensile tests was modelled and assigned to the FEA models (see Figure 7). Only the middle stretch of model (300 mm length) subjected to the three individual load cases was modeled. The FEA models followed exactly the dimension of the middle stretch of test specimens. Figure 8 shows the FEA models for control and perforated hollow cylinder together with the dimensions of the model as well as the perforations. 8-node quadrilateral thin shell element was used for the modelling of the cylindrical surface.

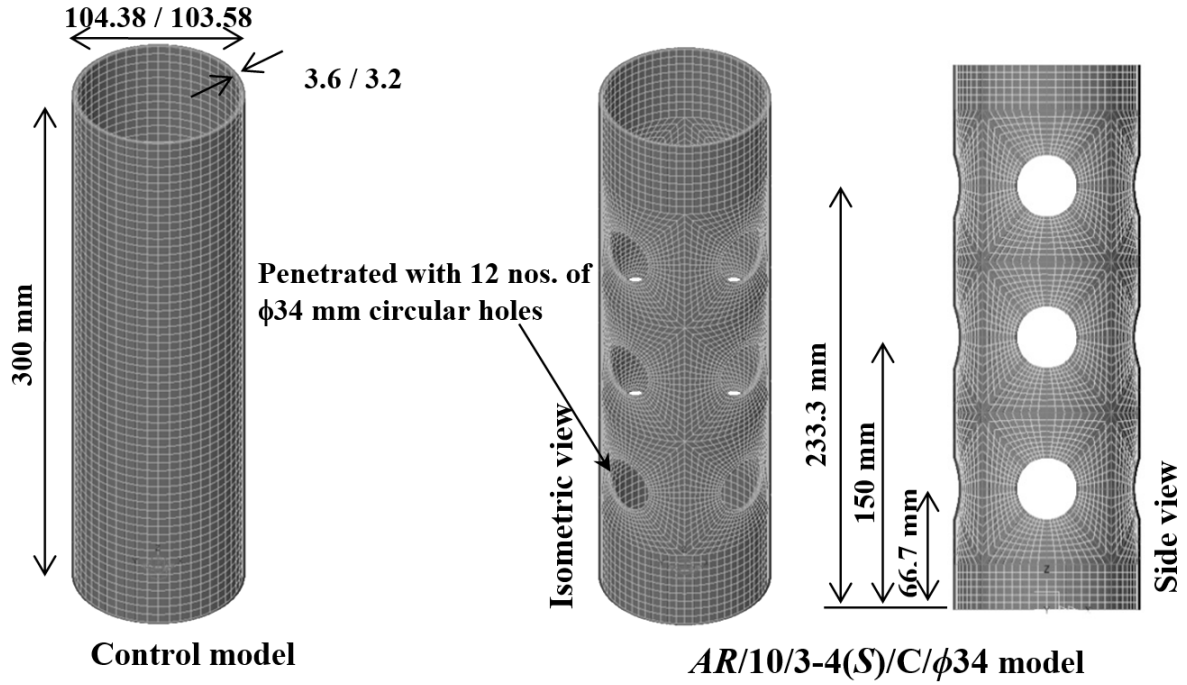

Figure 8: *FEA model for control and perforated hollow cylinder*

Support conditions assigned to the FEA models are: pinned at the bottom of circular hollow section for all the individual load case; pinned and released in longitudinal (z) axis at model top for compression load case; and free for all translational and rotational degree of freedoms at the top end for flexural and torsional load cases. Figure 9 shows the approach used to applied pure compression, flexural and torsional loads on the main circular hollow sections. A circular thick beam was connected to the top circumference of the circular hollow section with rigid link geometric constraint. Concentrated load was then applied at the top of the beam. Nonlinear analysis (material and geometrical) was carried out to obtain results for comparison with test results.

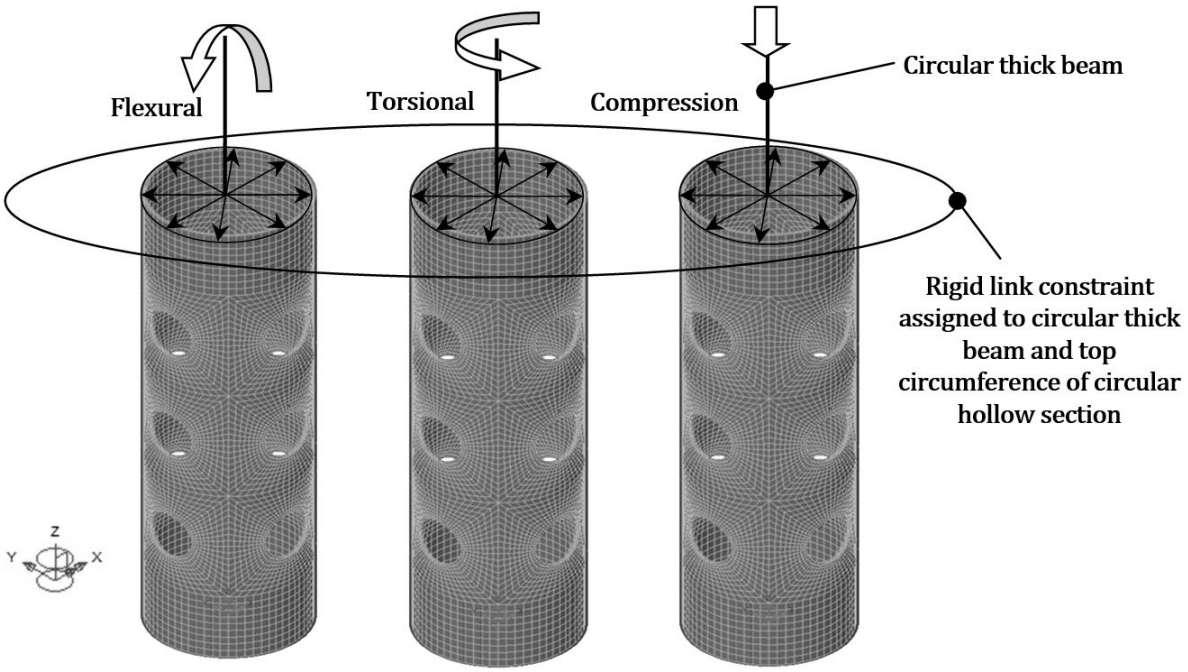

Figure 9: Approach used for load application on the FE models

4.2 Compression load case

Stress-strain relationship for FEA control and perforated models under compression load were plotted to compare the modulus of elasticity with the one obtained from tensile test. Both the control and perforated models show E and σ_y which are almost similar to the input values.

The force at yield stress for control model is used as the reference force, F_{ref} under compression load case. Graphs of F/F_{ref} vs. ε_z for control and perforated models were plotted and shown in Figure 10 and 11, respectively. Graphs *a*, *b*, and *c* for these two figures show curves of FEA models compared against the individual strain gauge for each test specimen. Snap back in strain reading (highlighted by '*' in Figure 11) for one particular strain gauge readings for perforated model CP01 and CP03 is noticed, while the remaining show increasing strains. Average strain curves were produced and shown in Figure 11(d).

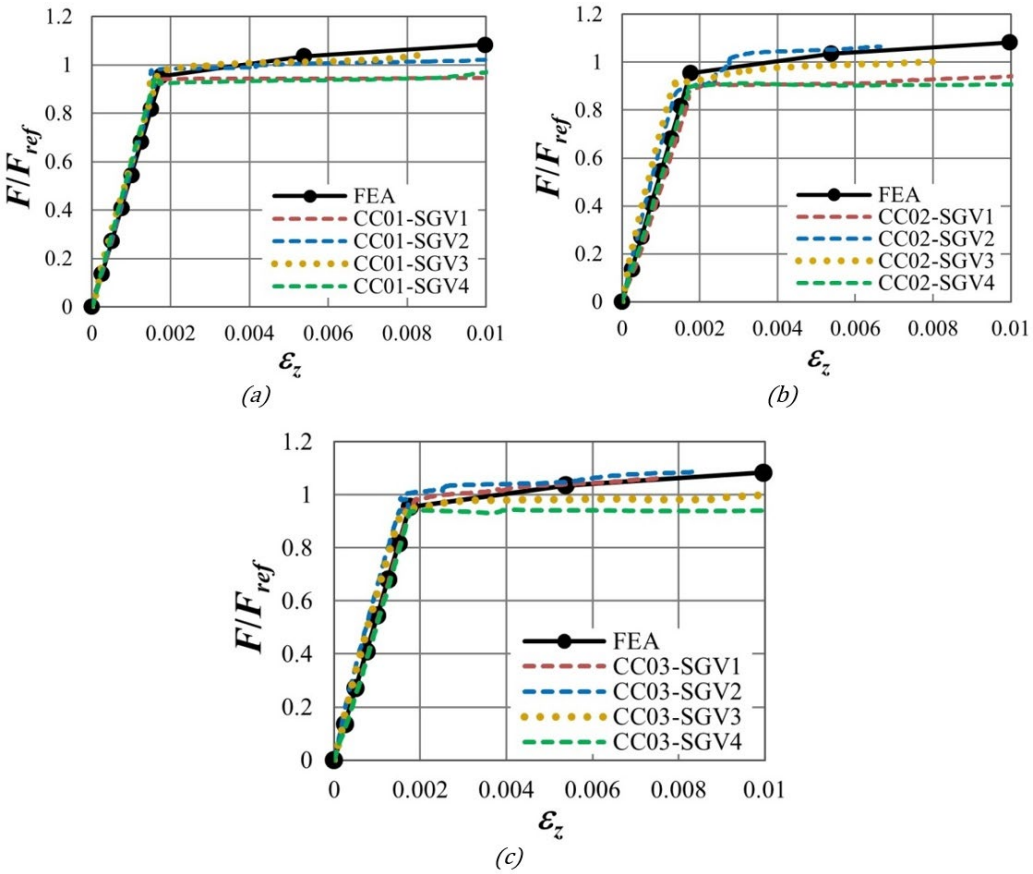

Figure 10: *Graphs of F/F_{ref} vs. ε_z for control models–compression test, (a) control model: CC01, (b) control model: CC02, (c) control model: CC03.*

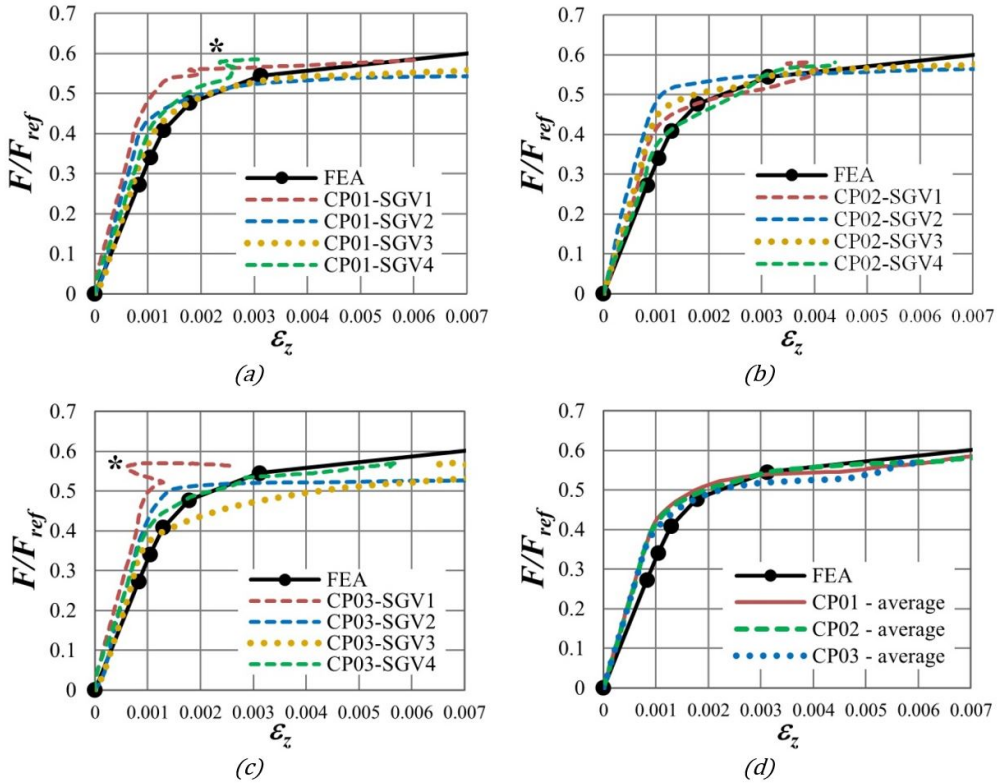

Figure 11: *Graphs of F/F_{ref} vs. ε_z for perforated models–compression test, (a) perforated model: CP01, (b) perforated model: CP02, (c) perforated model: CP03, (d) perforated model: average.*

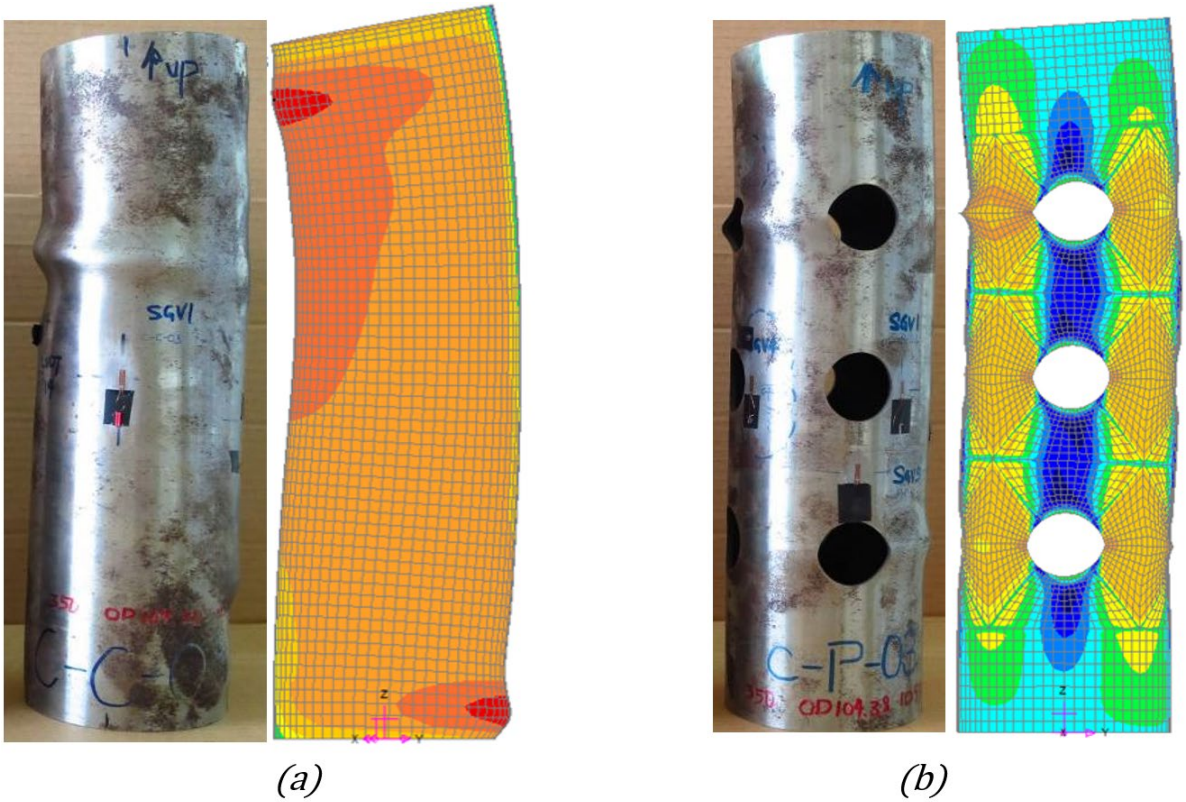

Figure 12**:** *Deformed shape of test specimen and FEA models under compression load with incorporated eccentricity, (a) control model, (b) perforated model.*

Both control and perforated FEA models produced F/F_{ref} - ε_z curves which correlate well with the test results. Perforated FEA model is found to show relatively larger difference from test results than the case of control model. FEA models show higher F/F_{ref} than test specimens in the plastic range.

The difference between FEA and test results might be due to imperfection in the test specimens. Slight unevenness either at the top or bottom edge of the test specimens was noticed. This could lead to minor tilt to the models and might results in minor bending during testing. Unavoidable small eccentricity during the setting up might occur and this leads to additional bending moment and hence, non-symmetrical test results. FEA models with incorporated small eccentricity (5mm from longitudinal axis) were analyzed and the deformed shapes are found to be agreeable with those observed in the test specimens as shown in Figure 12.

The inner surface was found to be uneven which affected the uniformity of thickness. This leads to unevenness in stress and strain distribution. A specific zone of a compression test control model was purposely assigned with smaller thickness in the FEA control model. The stress and strain contours have shown that the highest stress and strain were concentrated at regions with smaller thickness.

Reference markings for center and alignment were made as accurate as possible on the test specimen surface at all strain gauges positions. However, the strain gauges might have slight deviation from the desired alignments after installation and this could contribute to the difference between FEA and test results.

4.3 Flexural load case

The measured data obtained from the experimental test are the axial strains. For verification purpose, axial strains for FEA model were compiled and graphs of flexural moment (M) vs. ε_z (positive at tension surface and negative at compression surface) for control and perforated models were plotted and shown in Figure 13 and 14. The deformed shapes are shown in Figure 15. Good agreement was observed within linear range for M vs. ε_z graphs. FEA model shows slightly higher M than test specimen in the nonlinear range for the control model. M vs. ε_z curves for perforated FEA model however, lie within the average zone among the test specimen in the nonlinear range. The pattern of M vs. ε_z curves for perforated FEA model in the nonlinear range was also observed to agree well with test results. Close agreement was also noticed for the deformed shapes between test specimen and FEA models as shown in Figure 15.

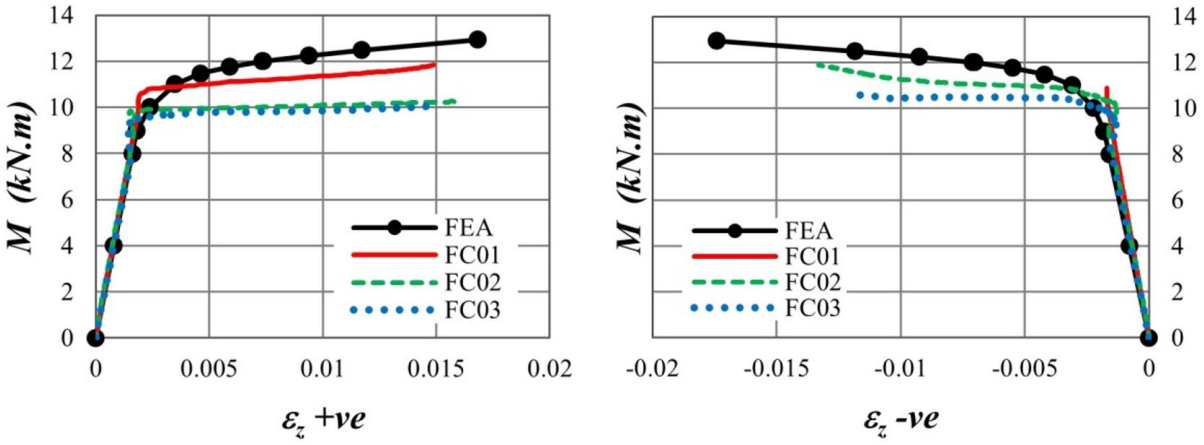

Figure 13: Graphs of M vs. ε_z for control models–flexural test.

The imperfection of the physical models due to fabrication and the unevenness of thickness at the inner surface are the possible reasons for the discrepancy between FEA and test results. Slight deviation from desired positions and alignments might happen to the strain gauges during installation and thus might have contributed to the discrepancies between test and FEA results.

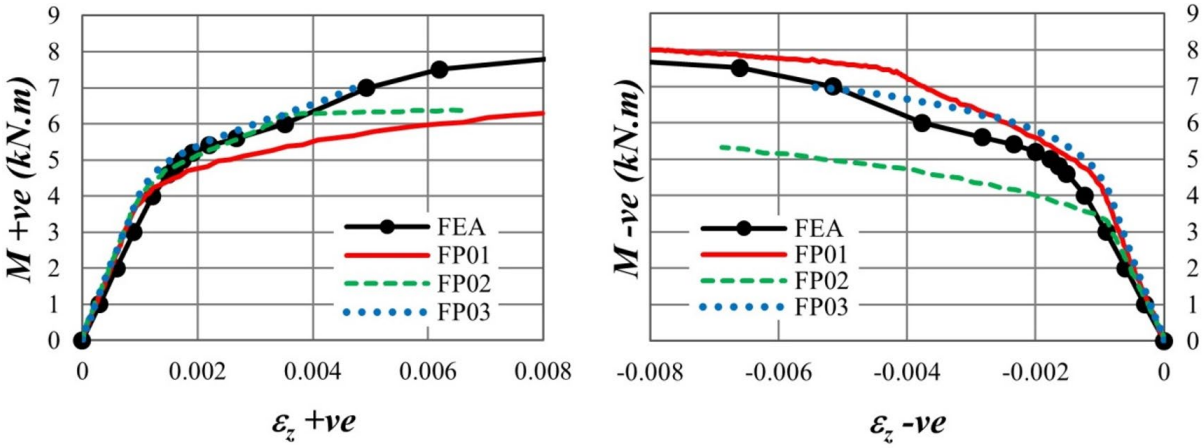

Figure 14: Graphs of M vs. ε_z for perforated models–flexural test.

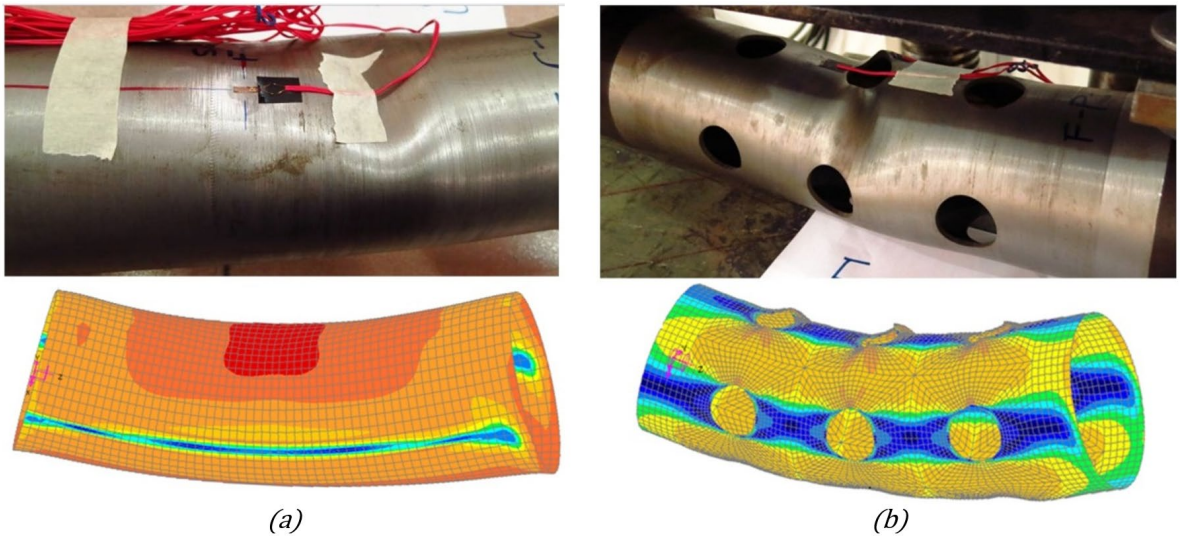

Figure 15: Deformed shapes for test specimen and FEA models under flexural load, (a) control model, (b) perforated model.

4.4 Torsional load case

Strain rosettes with 0°/45°/90° arrangement were installed on test specimen for torsional load tests. The rosettes were checked upon the components readings and the usable and unusable rosette readings were identified. All rosette readings for the control models (RT and RB for TC01 to TC03) are usable while only rosette RB for TP02 is usable for perforated models. Graphs of torsional moment (*T*) vs. strain for control models and perforated models are plotted and shown in Figure 16 and 17, respectively. The diagonally installed strain gauges (SGD1 and SGD2 - installed by assuming the principal strains oriented at approximately ±45°) were included in the graphs. The major and minor principle strains (ε_{p1} and ε_{p2}) between FEA and test results for control model correlate well within the elastic range. The torsional yield moments and the moments in nonlinear range for FEA model are noticed to be higher than test results.

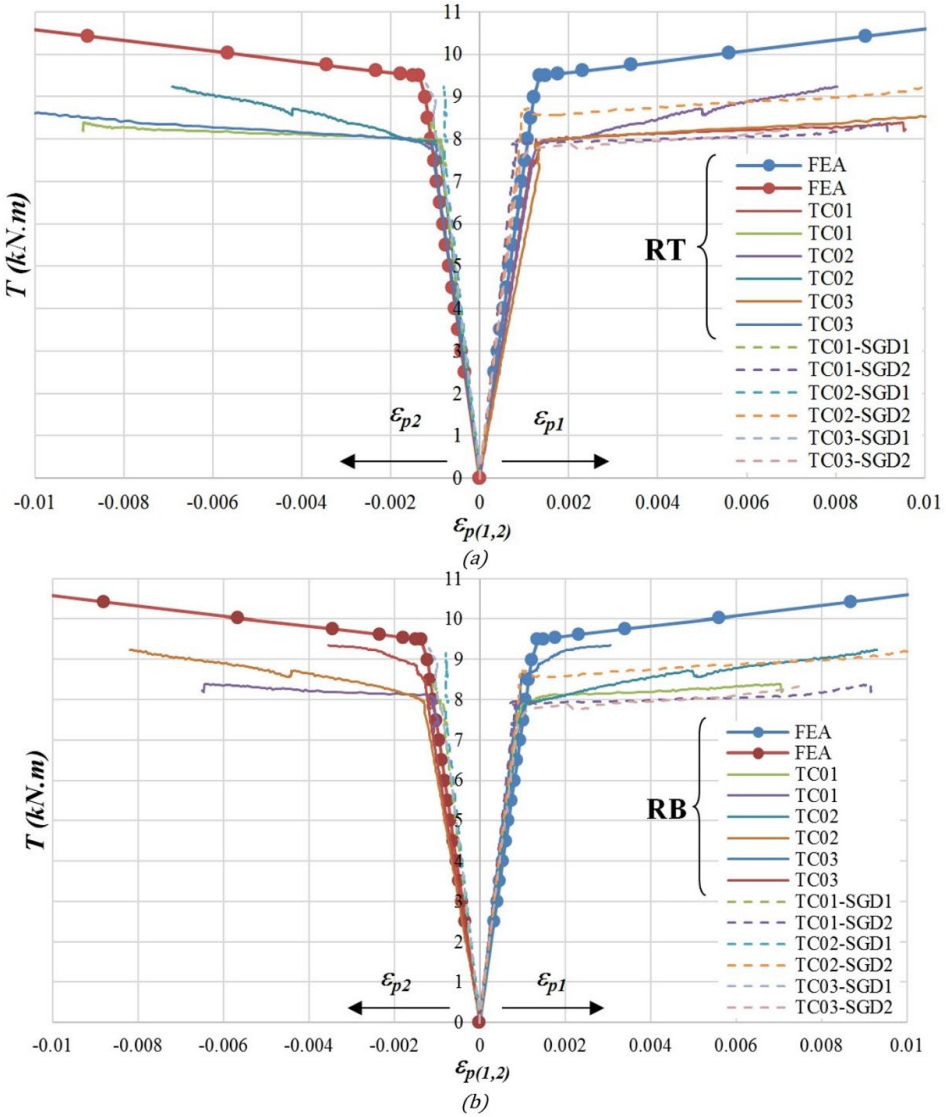

Figure 16: Graphs of torsional moment (T) vs. strain for experimental and FEA control models, (a) top strain rosette (RT), (b) bottom strain rosette (RB).

Only strain component readings of rosette RB from model TP02 are found acceptable and were used to obtain ε_{p1} and ε_{p2} for comparison with FEA results. ε_{p1} for this rosette however, only shows logical values but does not correlate well with FEA results. Readings for SGDs for test specimens correlate well with FEA results within the elastic range. Similar to those for control model, test specimens yielded at lower *T*. Deformed modes for test specimen and FEA models are shown in Figure 18 and both show considerably good agreement.

Strain rosettes and strain gauges might experience slight deviation from the reference lines on model surface or desired inclinations and locations. Marking reference lines on the curved surface for strain rosettes installation is much more difficult compared to for strain gauges. Installation process for strain rosettes is also the most difficult one especially at locations beside perforations and possibility for deviation to occur is also high. For the testing setup, friction also happens between of top plates of torsional arms and the loaders. Portion of applied force might be used to overcome the frictions. Combination of these might have contributed to the discrepancy between FEA and test results especially for perforated models specifically the strain rosette readings for TP02.

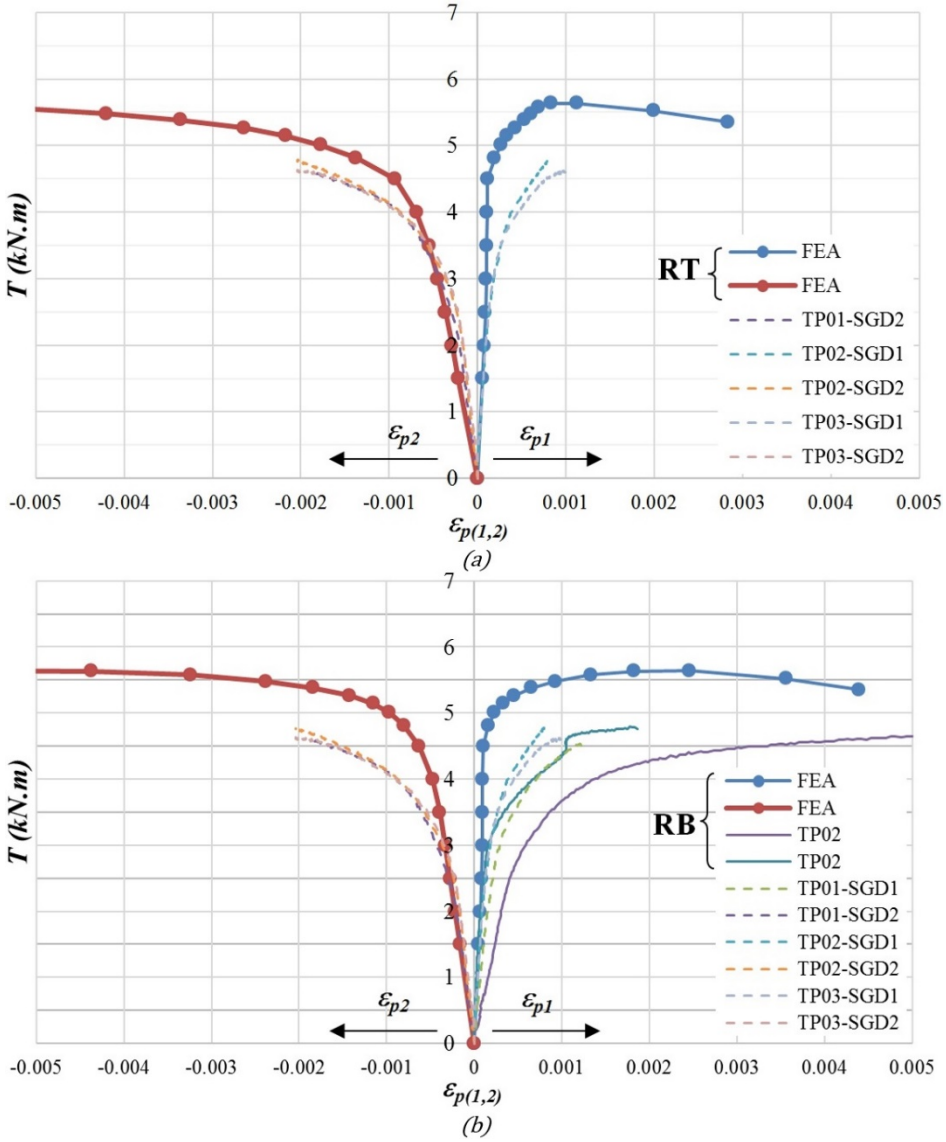

Figure 17: Graphs of torsional moment (T) vs. strain for experimental and FEA perforated models, (a) top strain rosette (RT), (b) bottom strain rosette (RB).

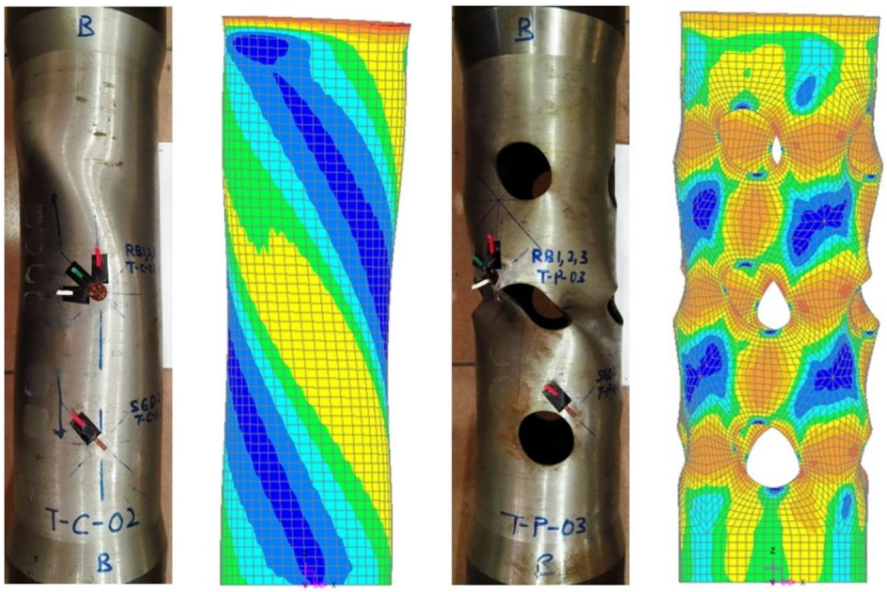

(a) *(b)*

Figure 18: Deformed shapes for test specimen and FEA models under torsional load, (a) control model, (b) perforated model.

5 CONCLUSIONS

For result comparison within the material linear range, FEA models generated using LUSAS show good agreement with test results for (i) compression and flexural load cases, and (ii) control models under torsional load case. For perforated models under torsional load, FEA results correspond well with the inclined strain gauge readings. The only available strain rosette results however, show significant discrepancy with the FEA and inclined strain gauge results. Deviation of strain gauges from the desired locations and inclinations, material and fabrication quality, and friction occurred in testing setup are possible causes causing the discrepancies between FEA and experimental results. The main focus of the numerical analysis is within the material linear range. Hence, the modeling approach is considered capable to produce reliable result for loading within the material linear range.

References

Cousseau, P., Schlax, M., Engelstad, R. L., Lovell, E. G. (1998, February). Natural frequencies of perforated cylindrical shells. In Proceedings of the 16th International Modal Analysis Conference 3243: 1054.

Degtyarev, V. V., Degtyareva, N. V. (2012). Elastic stability of uniformly compressed plates perforated in triangular patterns. Thin-Walled Structures 52: 165-173.

El-Sawy, K. M., Nazmy, A. S. (2001). Effect of aspect ratio on the elastic buckling of uniaxially loaded plates with eccentric holes. Thin-Walled Structures 39(12): 983-998.

FEA Ltd.(2005). LUSAS. User Manual, Version 13.7, in Surrey, UK

Ghazijahani, T. G., Jiao, H., Holloway, D. (2015). Structural behavior of shells with different cutouts under compression: An experimental study. Journal of Constructional steel research 105: 129-137.

Han, H., Cheng, J., Taheri, F., Pegg, N. (2006). Numerical and experimental investigations of the response of aluminum cylinders with a cutout subject to axial compression. Thin-Walled Structures 44(2): 254-270.

Jullien, J. F., Limam, A. (1998). Effects of openings of the buckling of cylindrical shells subjected to axial compression. Thin-Walled Structures 31(1-3): 187-202.

Kazuya. (2007). Posted on Yanko Design. Retrieved from http://www.yankodesign.com/.

Lane, T. (2009). O-14 Tower, Dubai: The Hole Story. Retrieved from http://www.building.co.uk/.

Maiorana, E., Pellegrino, C., Modena, C. (2009). Elastic stability of plates with circular and rectangular holes subjected to axial compression and bending moment. Thin-Walled Structures 47(3): 241-255.

Paik, J.K., (2007). Ultimate strength of perforated steel plates under edge shear loading. Thin-Walled Structures 45(3): 301-306.

Reiser, J., Umemoto, N. and Ocampo, J.M. (2010). Case study: O-14 folded exoskeleton. CTBUH Journal 3: 14-19.

Shanmugam, N. E., Thevendran, V., Tan, Y. H. (1999). Design formula for axially compressed perforated plates. Thin-Walled Structures *34*(1): 1-20.

Shariati, M., Dadrasi, A. (2012). Numerical and Experimental Investigation of Loading Band on Buckling of Perforated Rectangular Steel Plates. Research Journal of Recent Sciences 1(10): 63-71.

Shariati, M., Rokhi, M. M. (2008). Numerical and experimental investigations on buckling of steel cylindrical shells with elliptical cutout subject to axial compression. Thin-Walled Structures 46(11): 1251-1261.

Shariati, M., Rokhi, M. M. (2010). Buckling of steel cylindrical shells with an elliptical cutout. International journal of steel structures 10(2): 193-205.

The Agridulce Lookout House XPIRAL. (2009). Retrieved from http://www.archdaily.com/24024/agridulce-lookout-house-xpiral.

Trendir. (2009). Concrete shell structure eggshell – a concrete pod for all occasions. Posted on Trendir. Retrieved from http://www.trendir.com/.

Yeh, M. K., Lin, M. C., Wu, W. T. (1999). Bending buckling of an elastoplastic cylindrical shell with a cutout. Engineering Structures 21(11): 996-1005.